Electron-cyclotron-current-drive experiments in the DIII-D tokamak

R. A. James
Lawrence Livermore National Laboratory, Livermore, California 94550

G. Giruzzi, B. de Gentile, and L. Rodriguez
Association Euratom, Commissariat a l'Energie Atomique, Tore Supra, Cadarache, France

R. Harvey, J. Lohr, T. C. Luce, K. Matsuda, C. P. Moeller, R. Prater, and R. Snider
General Atomics, San Diego, California 92186-9784

A. Fyakhretdinov, Yu. Gorelov, and V. Trukhin
Kurchatov Institute, Moscow, U.S.S.R.

S. Janz
University of Maryland, College Park, Maryland 20742
(Received 3 May 1991)

Electron-cyclotron-current-drive (ECCD) experiments performed in the DIII-D tokamak have produced rf-driven currents of up to 100 kA. The experimental results, which exceed predictions using linear theory, are enhanced by the presence of a residual, toroidal dc electric field. These ECCD experiments are performed with plasma conditions sufficient to result in strong localized deposition of the rf power and good confinement of the rf-generated current carriers. These improved conditions permit a test of theory under reactor relevant conditions. Theoretical predictions obtained using a Fokker-Planck code are in good agreement with the experimental results when effects due to electron trapping and the residual dc electric field are included.

PACS number(s): 52.50.Gj, 52.25.Sw, 52.35.Hr, 52.55.Fa

Investigation of non-inductively-driven toroidal currents is an important topic within the field of magnetic-fusion energy research. Continuous or steady-state operation of a tokamak fusion reactor offers many engineering benefits [1]. In the case of electron-cyclotron-current-drive (ECCD), several specific advantages [2] make its use attractive for either fully or partially supporting the toroidal current in a tokamak. These advantages include the ability to remotely locate the rf sources, easily pass the rf power through the vacuum-vessel interface, and the capability to focus, aim, and efficiently deposit the microwave power at any internal location.

In this article, experimental results of the ECCD experiments performed in the DIII-D tokamak [3] and their comparison with theoretical predictions are presented and discussed. These experiments, performed with plasma conditions relevant to future machines, contrast with other ECCD experiments [4] in two important aspects. First, the measured rf-driven current is equal to or larger than the current predicted by linear theory [5], whereas experimental measurements from the other ECCD experiments are typically a factor of 2–3 times smaller than linear predictions. Second, the plasma conditions are significantly improved and permit a test of theory under reactor-relevant conditions. The DIII-D discharges are characterized by thermal-target plasmas with electron temperatures and densities sufficient to result in complete first-pass absorption and localized deposition of the rf power. In addition, the energy-confinement time (τ_E) is large compared to the expected slowing-down time of the rf-generated current carriers (τ_s). Both of these conditions are essential in obtaining good performance; strong localized deposition aids the formation of a high-energy electron tail and good confinement of these electrons improves the efficiency of ECCD. The absence of good energy confinement and/or insufficient first-pass absorption is attributed to the degraded performance obtained in the other efforts [4].

The physics of ECCD [5] can be understood as follows. When a resonant electron absorbs power from the rf wave, its perpendicular velocity increases with little or no change to its parallel velocity. As the total energy of the electron increases, its collision frequency decreases. Thus, over a time long compared to the collision rate, if this electron is well confined, it will contribute a larger amount of toroidal current ($j_e = -ev_\parallel$) than the equivalent electron that has not been heated. By selectively heating electrons moving in one toroidal direction, a net toroidal current results. The total momentum of the plasma is conserved as ions are preferentially dragged in the opposite direction.

The experimental parameters for the discharges discussed in this paper are the following. The plasma has a major radius $R_m \simeq 1.60$ m, a minor radius of $a \simeq 0.60$ m, and elongation of $\kappa \simeq 1.2$, and is limited on the inside

wall. The toroidal magnetic field is 2.14 T at $R_{res} \simeq 1.6$ m, placing the fundamental electron-cyclotron resonance at the center of the discharge. High-power microwaves (rf) at 60 GHz are generated by up to eight gyrotrons and transported to the tokamak in circular waveguide [6]. The rf is launched from the high-field side (inside wall) of the torus and polarized in the extraordinary (X) mode. The launching hardware is 0.13 m above the plasma midplane, and consists of several fixed reflectors, seven aimed at 15° and one aimed at 30° with respect to perpendicular injection. The antenna pattern is approximately a Gaussian beam with a 10° $1/e$ half-width. The rf power incident on the plasma is approximately 1 MW with pulse lengths up to 500 msec. Experimental profiles for the electron temperature $T_e(r)$, electron density $n_e(r)$, and $Z_{eff}(r)$ are determined using electron-cyclotron emission, CO_2 interferometry, and visible bremsstrahlung emission. Discharges with a fixed toroidal current (I_P) between 300 and 500 kA are used.

The experimental calculation of the rf-driven current I_{rf} is complicated by the presence of a non-zero-loop voltage during the rf phase. This residual voltage $V_l(\mathrm{rf})$ is the result of having insufficient electron-cyclotron-heating (ECH) power to drive all of the toroidal current and of using feedback control to keep the total toroidal current I_P constant. Under these conditions, the steady-state circuit equation for the plasma current becomes

$$I_P = I_{rf} + I_{BS}(\mathrm{rf}) + \frac{V_l(\mathrm{rf})}{R_P(\mathrm{rf})} , \tag{1}$$

where $I_{BS}(\mathrm{rf})$ is the bootstrap current [7] and $R_P(\mathrm{rf})$ is the plasma resistance during the rf phase. Using a one-dimensional numerical code, $R_P(\mathrm{rf})$ and I_{BS} are calculated using the experimental profiles for $T_e(r)$, $n_e(r)$, and $Z_{eff}(r)$. The plasma resistance is calculated assuming power balance and toroidal symmetry; $R_P(\mathrm{rf}) = (2\pi R_m / I_\Omega^2) \int \eta_\parallel(r) J_\Omega^2(r) r\, dr$, where $\eta_\parallel$ is neoclassical resistivity, $J_\Omega = J_{total} - J_{BS}$ is the Ohmic current density, J_{total} is determined from magnetics, and $I_\Omega = 2\pi \int J_\Omega(r) r\, dr$.

We now define V_l^* as the loop voltage that is expected during the rf phase if $I_{rf}=0$, i.e., $V_l^* = [I_P - I_{BS}(\mathrm{rf})] R_P(\mathrm{rf})$. Since the magnitude of V_l^* is determined by the plasma resistance, this voltage is referred to as the "resistive" voltage of the plasma. Using this definition, Eq. (1) can be recast as

$$I_{rf} = [I_P - I_{BS}(\mathrm{rf})] \left[\frac{V_l^* - V_l(\mathrm{rf})}{V_l^*} \right] . \tag{2}$$

The validity of the numerical calculation of the plasma resistance is demonstrated in the Ohmic phase. On average, the numerical calculations of the plasma's resistive voltage during the Ohmic phase, $V_l^*(\mathrm{Oh.}) = [I_P - I_{BS}(\mathrm{Oh.})] R_P(\mathrm{Oh.})$, agree within ±5% of the experimental measurements. As a result of this strong systematic agreement, the experimental error bars during the rf phase are determined by assuming a ±5% error in the calculation of $V_l^*(\mathrm{rf})$. Note that through the use of Eq. (2), the error in I_{rf} is substantially larger. In addition, this error exceeds the error that results from inaccuracies in the determination of the experimental profiles.

The time history of relevant plasma parameters for a typical discharge is shown in Fig. 1. The existence of a stationary state is indicated by the essentially steady-state values of T_e, n_e, and R_m during the majority of the ECH pulse. For this discharge, the numerically calculated resistive loop voltage, during the rf phase, is $V_l(\mathrm{rf}) \simeq 0.38$ V. With an experimental loop voltage of $V_l(\mathrm{rf}) \simeq 0.32$ V and $I_P = 400$ kA, an rf-driven current of $I_{rf} \simeq 63 \pm 17$ kA is calculated. During the Ohmic phase, the calculated resistive loop voltage of $V_l^*(\mathrm{Oh.}) \simeq 0.63$ V is within 3% of the experimental value. The numerical calculations of the bootstrap current are approximately 20 kA during the Ohmic phase and 31 kA during the rf phase. In general, during the rf phase the electron-temperature profiles become more peaked, the electron-density profiles become flatter, and Z_{eff} increases across the profile. For different discharges, central values for these parameters vary over the following ranges: $2.0 < T_e(\mathrm{keV}) < 3.6$, $1.0 < n_e(10^{19}/\mathrm{m}^3) < 2.0$, and $2.5 < Z_{eff} < 5.5$. The magnitude of the loop voltage during the rf phase is between 0.22 and 0.45 V.

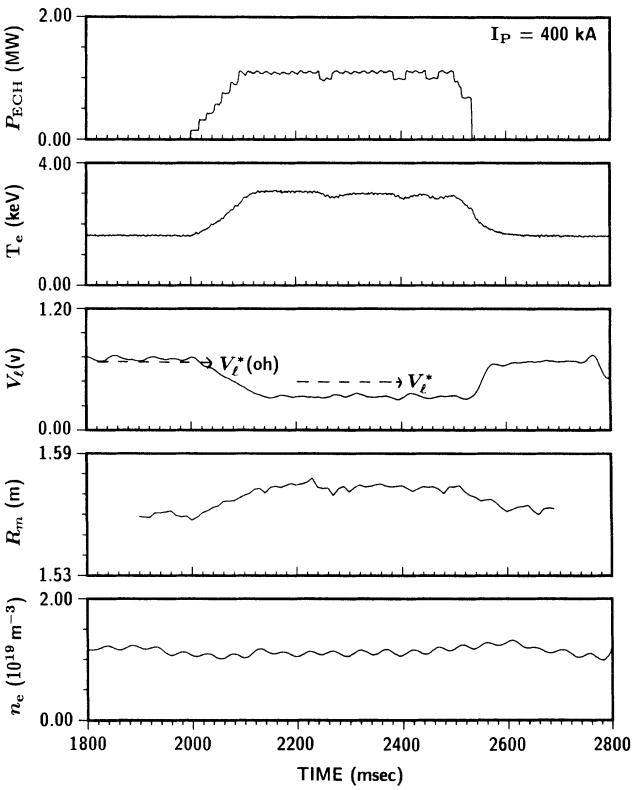

FIG. 1. Time history of plasma parameters: (a) electron-cyclotron-heating (ECH) power level in megawatts (MW), (b) central electron temperature from ECE, in keV, (c) loop voltage near the plasma surface in volts (V), (d) radial position of the magnetic center of the plasma in meters (m), and (e) the line-averaged electron density in $10^{19}/\mathrm{m}^3$. The staircase behavior at the beginning of the ECH pulse results from the sequential timing used for turning on the gyrotrons. The numerical calculations of the "resistive" voltages $V_l^*(\mathrm{Oh})$ and V_l^*, during both the Ohmic and rf phases are shown as dashed lines in part (c).

In Fig. 2, data are shown which demonstrate that I_{rf} is driven in the intended direction. In this figure the quantity $[V_l^* - V_l(\mathrm{rf})]/V_l^*$, which represents the relative difference between the predicted and measured loop voltage, is plotted for both coinjection and counterinjection discharges. For coinjection, the rf is launched in the same direction in which the toroidal current I_P is directed. Counterinjection is accomplished by reversing the direction of I_P. The behavior illustrated in this figure is explained by noting that for coinjection, I_{rf} should aid I_P. Thus with I_P held constant, $V_l(\mathrm{rf})$ should be less than V_l^*. In contrast, for counterinjection, I_{rf} should oppose I_P, thus $V_l(\mathrm{rf})$ should be greater than V_l^*.

As will be discussed next, the residual, toroidal (parallel) dc electric field $E_\parallel = V_l(\mathrm{rf})/2\pi R_m$ strongly enhances the rf-driven current. Experimentally, $E_\parallel/E_{cr}$ reaches a maximum of 40%. $E_{cr} \simeq n_e(10^{19})(Z_{eff}+2)/8\pi T_e(\mathrm{keV})$ is the critical field [8] for runaway of thermal electrons. Under these conditions, a linearized theoretical treatment [9] of the experimental data is not adequate. Thus, in order to quantitatively model the experiment, we rely upon a detailed Fokker-Planck code [10]. The code is fully relativistic, bounced-averaged, and accounts for effects resulting from trapped electrons and the presence of a parallel dc electric field. The code is coupled to a ray-tracing code, using 45 rays to represent the launched antenna patterns. Using the experimental profiles for $T_e(r)$, $n_e(r)$, and $Z_{eff}(r)$ as inputs, a steady-state calculation of $f_e(v_\parallel, v_\perp, r)$ is performed. Calculations of the local rf damping are self-consistent with the distorted electron-velocity distribution. At low rf power levels and with effects due to electron trapping and $E_\parallel$ turned off, the computational results are in agreement with Fisch-Boozer theory [5]. When effects due to trapped electrons are turned on, the computational results are in agreement with the appropriate analytic theory [11].

In Fig. 3, the experimental measurements of I_{rf}/P_{rf} are plotted as a function of $T_e/n_e(Z_{eff}+5)$. This parameter, which is derived from linear theory [5], describes the functional dependence of the plasma parameters which influence the rf current-drive efficiency. In deriving this

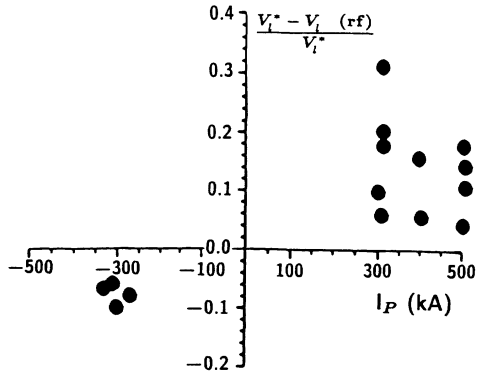

FIG. 2. The magnitude of the quantity $[V_l^* - V_l(\mathrm{rf})]/V_l^*$ vs I_P. Coinjection discharges are with positive values of I_P. For a fixed I_P, the data variation results from operation with different electron temperatures and densities.

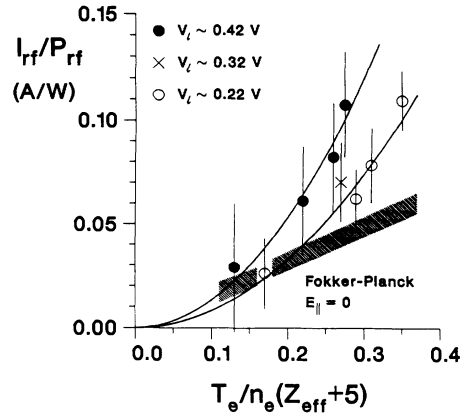

FIG. 3. Experimental measurements of I_{rf}/P_{rf} vs the central value of $T_e/n_e(Z_{eff}+5)$. The experimental data are grouped according to its approximate residual-loop voltage and for $V_l(\mathrm{rf}) \simeq 0.42$ and 0.22 V, is fitted with a parabolic curve. Fokker-Planck calculations for each discharge, with $E_\parallel = 0$ fall within the shaded region. The width of this region results from having used the measured profiles.

parameter, the normalized resonant velocity $v_\parallel/v_{th}$ is assumed to be approximately constant, an assumption supported by our Fokker-Planck code for these experimental conditions. The $(Z_{eff}+5)$ term results from current dissipation via drag and pitch-angle scattering [5]. For each discharge, the Fokker-Planck prediction with $E_\parallel = 0$ falls within the shaded region in Fig. 3. As can be seen, the experimental measurements are equal to or greatly exceed the computational predictions. Electron trapping has been included in these computations because the deposition profiles, calculated by the Fokker-Planck code are peaked off axis; thus some degradation of the current-drive efficiency by trapped electrons is to be expected [11]. With electron trapping turned off, the Fokker-Planck computations, which increase by between 40% and 60%, are also inconsistent with the experimental data.

The influence of the residual dc electric field is illustrated by grouping the experimental data according to the approximate value of the residual-loop voltage. As depicted in Fig. 3, the experimental data for $V_l(\mathrm{rf}) \simeq 0.42$ and 0.22 V appear to scale as the square of $T_e/n_e(Z_{eff}+5)$. This effect is postulated to be the result of the fact that for a fixed-loop voltage $E_\parallel/E_{cr} \propto T_e/n_e(Z_{eff}+2)$. Thus the measured rf-driven current is the product of the linear current and a parallel dc electric-field enhancement. In addition, under conditions for which linear theory would predict essentially the same rf-driven current, the four discharges clustered around $T_e/n_e(Z_{eff}+5) \simeq 0.27$ demonstrate that I_{rf}/P_{rf} increases as $E_\parallel/E_{cr}$ increases, $I_{rf}/P_{rf} = 0.06$, 0.07, 0.08, and 0.11 (A/W) corresponding to $E_\parallel/E_{cr} = 0.24$, 0.32, 0.38, and 0.41.

In Fig. 4, the experimental measurements of I_{rf} are compared to the Fokker-Planck predictions with $E_\parallel = V_l(\mathrm{rf})/2\pi R_m$. Good agreement, as illustrated in this figure, is obtained only when effects due to electron

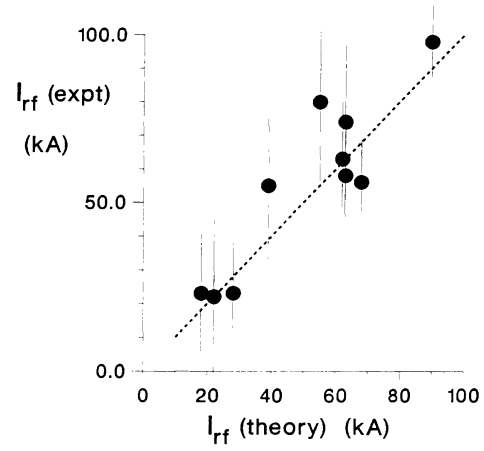

FIG. 4. The experimental measurements of I_{rf} vs the Fokker-Planck code calculations of I_{rf}. Both electron trapping and the experimental values of $E_{\|}$ are included in the computational calculations. The dotted line represents perfect agreement.

trapping and $E_{\|}$ are included. Thus we conclude that these aspects of the kinetic theory of ECCD are verified.

Several additional agreements exist between the Fokker-Planck calculations and the experimental results. First, for the more robust discharges, the steady-state electron-velocity distribution function, calculated by the Fokker-Planck code, indicates a strong distortion of electron velocities between $2 < v/v_{th} < 5$. Energetic electrons with these energies are observed by several diagnostics, including an energy-resolving hard-x-ray detector and electron-cyclotron emission (ECE). In these plasmas, the calculated slowing-down time (τ_s) for electrons with these velocities is between 0.3 and 5 msec. This is much smaller than the experimental energy confinement time (τ_E) of ~ 30 msec, indicating that these electrons should be well confined. As stated earlier, good confinement is essential for maximizing the rf current-drive efficiency since I_{rf} appears on the time scale of τ_s. Second, the Fokker-Planck code predicts that the first-pass absorption is essentially 100% and that both the rf deposition profile and the resulting rf-driven current are localized off axis, inboard of the midplane between about 1.40 and 1.55 m. With I_P held constant, the current profile should broaden and the central current density should decrease. For discharges with sawteeth present, the temporal behavior of signals from the soft-x-ray diode array show that the inversion radius ($q=1$) has contracted during the rf phase, indicating a broadening of the current profile.

As a final comment, Fig. 3 shows that an increase in I_{rf} and thus an increase in the rf current-drive efficiency results when a toroidal electric field is present. In addition to Ohmic induction, toroidal electric fields will be generated during plasma initiation and current-profile modifications. Although these electric fields will decay with time, the resulting current-drive enhancement makes it important to include their effects in predicting results.

In summary, ECCD experiments in the DIII-D tokamak have successfully produced rf-driven currents of up to 100 kA. The plasma conditions result in strong localized deposition of the rf power and good confinement of the rf-generated current carriers. Systematic loop voltage behavior for coinjection and counterinjection discharges confirm that I_{rf} is driven in the expected direction. Good agreement is obtained between the experimental measurements and the theoretical predictions using a Fokker-Planck code which includes nonlinear effects due to electron trapping and the residual dc electric field. The strong agreement between theory and experiment serves to verify these aspects of the kinetic theory of ECCD.

The authors would like to thank the DIII-D operations group for their diligent efforts in performing these experiments. Those authors who are visitors at the DIII-D facility are also appreciative of the hospitality and cooperation afforded by the staff of General Atomics in executing these experiments and analyzing their results. This work is sponsored by the U.S. Department of Energy under Contract Nos. DE-AC03-89ER51114 and W-7405-ENG-48.

[1] J. R. Gilleland *et al.*, Nucl. Fusion **29**, 1191 (1989).
[2] R. Prater, *Eighth Topical Conference on Radio-Frequency Power in Plasmas,* AIP Conf. Proc. No. 190 (AIP, New York, 1989), p. 22.
[3] J. L. Luxon and L. G. Davis, Fusion Technol. **8**, 441 (1985).
[4] D. F. H. Start *et al.*, Phys. Rev. Lett. **48**, 624 (1982); H. Tanaka *et al.*, *ibid.* **60**, 1033 (1988); B. Lloyd *et al.*, Nucl. Fusion **28**, 1013 (1988); V. Erckmann *et al.*, Eur. Phys. Soc. Conf. Amsterdam **14b**, III 1271 (1990); V. V. Alikaev *et al.*, Eur. Phys. Soc. Conf. Berlin **15c**, III 361 (1991).
[5] N. J. Fisch, Rev. Mod. Phys. **59**, 175 (1987); N. J. Fisch and A. H. Boozer, Phys. Rev. Lett. **45**, 720 (1980).
[6] C. P. Moeller, Fusion Technol. **15**, 725 (1989).
[7] S. P. Hirshman and D. J. Sigmar, Nucl. Fusion **21**, 1079 (1981).
[8] H. Knoepfel and D. A. Spong, Nucl. Fusion **19**, 785 (1979).
[9] N. J. Fisch, Phys. Fluids **28**, 245 (1985).
[10] G. Giruzzi *et al.*, Eur. Phys. Soc. Conf. Berlin **15c**, III 365 (1991); G. Giruzzi, Phys. Fluids **31**, 3305 (1988); R. L. Meyer, G. Giruzzi, and V. Krivenski, Comput. Phys. Commun. **40**, 153 (1986).
[11] G. Giruzzi, Nucl. Fusion **27**, 1934 (1987).